Journal of Wind Engineering and Industrial Aerodynamics, 37 (1991) 255–268
Elsevier Science Publishers B.V., Amsterdam — Printed in The Netherlands

On aerodynamic sealing for industrial applications

L.A. Oliveira and J.J. Costa

Dep. Engenharia Mecânica, Universidade de Coimbra, Largo D. Dinis, 3000 Coimbra, Portugal

M.G. Carvalho

Dep. Engenharia Mecânica, Universidade Técnica de Lisboa, Av. Rovisco Pais, 1096 Lisbon, Portugal

H.J. Gerhardt and C. Kramer

Fachhochschule Aachen and Ingenieurgemeinschaft WSP, Welkenrather Strasse 120, D-5100 Aachen, Germany

(Received June 4, 1990)

Summary

This paper describes a new device for aerodynamic sealing of openings for the passage of strip-like material in chambers, e.g. in industrial furnaces, dryers, and for clean rooms. A numerical prediction procedure for the flow generated by the sealing device is presented. The influence of the relevant flow parameters upon the sealing efficiency is systematically analysed. Theoretical predictions are validated through concentration measurements in a physical model of a strip flotation furnace. The advantages of the new device—contactless sealing and minimized leakage of the atmosphere from inside the chamber to be sealed—are discussed in detail.

1. Introduction

When direct contact between solid surfaces is to be avoided, mechanical sealing of a compartment with a special gas atmosphere is frequently not suitable. Aerodynamic sealing is then a very attractive alternative.

For many applications in industrial heat treatment, the furnaces used have openings where the material to be heat-treated is continually fed through. If the goods under consideration have sensitive surfaces, the usual sealing devices like curtains or brushes must not be used. In such cases, a contactless sealing consisting of gas curtains is necessary. For many applications the mixing of furnace and ambient atmosphere has to be prevented. This is essential if, for example, penetration of oxygen into the furnace must not occur either for safety reasons or due to the constraints of the heat treatment process. For sealing purposes, plane jets, so-called jet curtains, are currently used as aerodynamic sealing. Because of the turbulence generated by the jet flow, a rather intense

0167-6105/91/$03.50

mixing between the jet curtain and the ambient will occur. Thus, to prevent oxygen penetration, the jet curtain has to be adjusted in such a way that most of the furnace gas used for sealing purposes will leave through the opening and will be lost.

The literature gives little, and mainly experimental, information concerning jet sealing devices for compensating pressure differences (see Esteban and de Verdier [1] and Kuster [2]). In a fundamental investigation, Kuster showed that the plane jets are highly suitable devices to compensate for pressure differences, but their use as concentration sealing is very limited. A concentration sealing may only be achieved if the nozzle is close enough to the goods fed through the furnace openings, so that the jet core reaches the goods. Even for such arrangements, the loss of furnace atmosphere is appreciably high. El-banna and Sabbagh [3] have presented measurements of mean static pressure and mean and fluctuating velocities of the flow field, generated by the interaction between two parallel two-dimensional jets. The effects of the velocity of the two jets on the flow field was studied, and they concluded that the axis of the combined jet comes closer to the power jet as the velocity of the weak jet decreases.

The present paper reports the main results of a theoretical and experimental study which is in a way a continuation of the fundamental study of Kuster. The emphasis of the follow-up work is on the development of a concentration sealing device where the above-mentioned problems are overcome [4].

2. Description of the concentration sealing device

To avoid mixing between ambient and furnace atmosphere the commonly used plane jet arrangement was modified. The plane jet is divided into two parts, as shown in Fig. 1. One half-nozzle is fed by the furnace atmosphere, the other by a sealing gas, e.g. N_2 or air. Mixing between the furnace atmosphere and the sealing gas may only occur at the interface of the two half-jets. If the exit velocity of both half-jets is almost equal, mixing may only happen due to diffusion. Since the diffusion velocity is much smaller than the jet velocity, the mixing is very small and may be negligible for many applications. Critical situations will occur if the heat treatment process demands a furnace atmosphere consisting of hot hydrogen. To have a stable jet, the centreline of which is perpendicular to the goods passing through the opening, the momentum of the two half-jets has to be equal. This will lead to higher exit velocities of the half-jet supplied by the furnace gas. If, for example, H_2 at a temperature of 700 K is used as the furnace atmosphere and N_2 at 10 m s^{-1} and 300 K as the sealing gas, the difference in exit velocity for those two gases is roughly 30 m s^{-1}. Therefore, the two half-jets will lead to a slip stream with mixing at their centreplane.

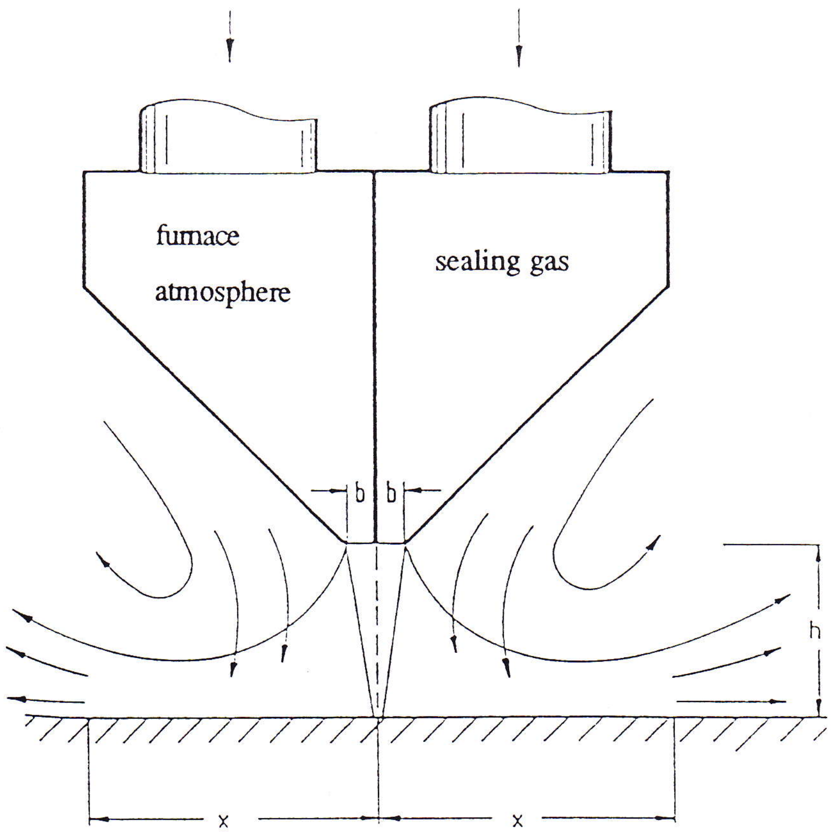

Fig. 1. Schematic of the new sealing device with divided nozzle.

3. Mathematical model

The flow geometry considered for the theoretical study is shown in Fig. 2. The two plane parallel jets are originated by a divided nozzle with a width of $2b$ (b=5 mm). Fluids 1 and 2 enter through the divided nozzle with velocities V_1 and V_2, respectively. The nozzle is facing a normal wall at a distance h from its exit. Air/air, air/N_2 and H_2/N_2 jets are analysed for different inlet conditions and different values of $h/2b$.

The governing transport equations of steady two-dimensional turbulent flow were applied in their cartesian coordinate form. The time-averaged equations for the conservation of momentum are in compact tensor notation, as follows:

$$\frac{\partial}{\partial x_j}\left(\bar{\rho}U_j U_i+\bar{p}\delta_{ij}-\mu\left[\frac{\partial U_i}{\partial x_j}+\frac{\partial U_j}{\partial x_i}-\frac{2}{3}\frac{\partial U_k}{\partial x_k}\delta_{ij}\right]\right)+(\bar{\rho}-\rho_{\mathrm{ref}})g_i$$

$$+\frac{\partial}{\partial x_j}(\bar{\rho}\overline{u'_j u'_i})=0 \qquad (1)$$

where U_i and u'_i are the mean and fluctuating velocity components in the x_i direction, ρ is density, ρ_{ref} a reference value, g_i is the magnitude of the gravitational acceleration in the i direction, p is pressure, μ is the laminar viscosity,

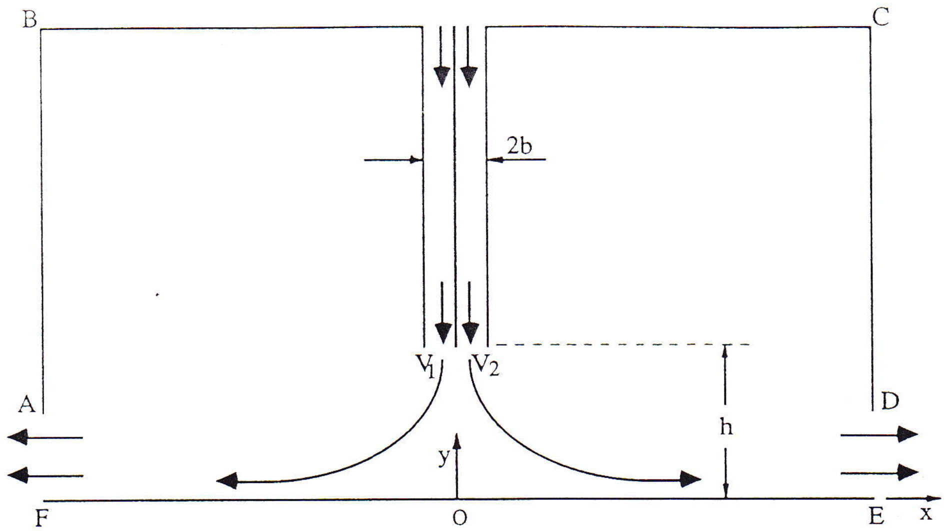

Fig. 2. Flow geometry and computational domain. $b=5$ mm, $BC=1$ m, $FB=0.45$ m.

and the operator δ_{ij} is unity for $i=j$ and zero when $i\neq j$. The overbar denotes mean values.

The transport equation for the mass fraction of component 1, c_1, is given by

$$\frac{\partial}{\partial x_j}(\bar{\rho}U_j c_1)-\frac{\partial}{\partial x_j}\left(\Gamma_{c1}\frac{\partial c_1}{\partial x_j}\right)=0 \tag{2}$$

The mass fraction of component 2 is given by

$$c_2=1-c_1 \tag{3}$$

In addition to eqns. (1)–(3) we must also include the equation of mass continuity:

$$\frac{\partial}{\partial x_i}(\bar{\rho}U_i)=0 \tag{4}$$

The "two-equation" turbulence model of Jones and Launder [5], in which equations for the kinetic energy of turbulence, K, and its dissipation rate, ϵ, are solved, was considered appropriate. The correlations in eqn. (1) are expressed, in analogy with laminar flow, as

$$-(\overline{\bar{\rho}u_j'u_i'})=\mu_t\left(\frac{\partial U_i}{\partial x_j}+\frac{\partial U_j}{\partial x_i}-\frac{2}{3}\frac{\partial U_k}{\partial x_k}\delta_{ij}\right) \tag{5}$$

where μ_t is a "turbulent" viscosity that may be related to K and ϵ by dimensional arguments:

$$\mu_t=c_\mu\rho K^2/\epsilon \tag{6}$$

where c_{μ} is a constant of the model. The turbulent exchange coefficient, $\Gamma_{\phi,\mathrm{t}}$, for any variable ϕ may be expressed as

$$\Gamma_{\phi,\mathrm{t}} = \mu_{\mathrm{t}}/\sigma_{\phi,\mathrm{t}} \tag{7}$$

where $\sigma_{\phi,\mathrm{t}}$ is a turbulent Prandtl number of order unity.

The differential equations for K and ϵ that the authors have solved are

$$\frac{\partial}{\partial x_j}(\bar{\rho}U_jK) - \frac{\partial}{\partial x_j}\left(\Gamma_K\frac{\partial K}{\partial x_j}\right) - \mu_{\mathrm{t}}\frac{\partial U_i}{\partial x_j}\left(\frac{\partial U_i}{\partial x_j}+\frac{\partial U_j}{\partial x_i}\right) + \bar{\rho}\epsilon = 0 \tag{8}$$

$$\frac{\partial}{\partial x_j}(\bar{\rho}U_j\epsilon) - \frac{\partial}{\partial x_j}\left(\Gamma_\epsilon\frac{\partial \epsilon}{\partial x_j}\right) - C_1\frac{\epsilon}{K}\mu_{\mathrm{t}}\frac{\partial U_i}{\partial x_j}\left(\frac{\partial U_i}{\partial x_j}+\frac{\partial U_j}{\partial x_i}\right) + C_2\bar{\rho}\frac{\epsilon^2}{K} = 0 \tag{9}$$

where C_1 and C_2 are further constants and Γ_K and Γ_ϵ are determined via eqn. (7). The standard constants of the model were used (Launder and Spalding [6]).

The density was determined from the equation of state:

$$\rho = p\cdot[R_0T/M]^{-1} \tag{10}$$

where p is pressure, R_0 is the universal gas constant and M is the average molecular weight of the mixture.

4. Numerical solution procedure

The partial differential equations were discretized using the finite volume method (see Gosman and Pun [7]). The approximation of the convective fluxes applied at each control volume face was performed using the hybrid central/upwind difference scheme (Spalding [8]). The velocities and pressures were calculated by a variant of the SIMPLE algorithm described in the work of Caretto *et al.* [9]. The solution of the individual equation sets was obtained by a Gauss–Seidel line-by-line iteration.

The computational domain was bounded by impermeable walls, *ABCD* and *EF*, with two flow exits, *AF* and *DE*, as shown in Fig. 2. The walls and the flow exits were located far enough from the nozzle to ensure that they did not significantly affect the flow in the region of interest. At the outflow boundary, all

TABLE 1

Flow configurations used for numerical predictions

Fluid 1/fluid 2	$h/(2b)$	V_1 (m s^{-1})	V_2 (m s^{-1})
H_2/N_2	1.6, 2.8, 4.6, 5.6	10, 37.3	10
Air/N_2	1.6, 2.8, 4.6, 5.6	10	10
Air/Air	1.6, 2.8, 4.6, 5.6	10	10

the dependent variables were governed by a zero-gradient condition. The velocity boundary conditions at the solid walls were those of zero tangential and normal components. The domain considered was mapped by a nonuniform mesh having small size cells in regions with pronounced gradients. A grid of 52×42 nodes along the horizontal and vertical directions, respectively, was used, although negligible differences were observed between the solutions obtained with this grid and with one of 42×32 nodes. Convergence was attained when the normalized residuals for the three equations of momentum and mass conservation were less than 5×10^{-3}. This was achieved after 5000 iterations, which corresponds to 3 h 50 min CPU time on a VAX 8530.

The flow configurations investigated are listed in Table 1. The velocity V_2 is kept constant and equal to 10 m s^{-1} and was taken as a reference value for the stream function normalization. The velocity V_1 is chosen to ensure that the two half-jets have the same flux momentum at the nozzle exit, except for the case H_2/N_2 where for comparative reasons the two conditions (equal flux momentum and equal velocities) were considered.

5. Experimental apparatus

The efficiency of the sealing device was also experimentally investigated in combination with a physical model of a strip flotation furnace. Figure 3 shows a schematic of the arrangement.

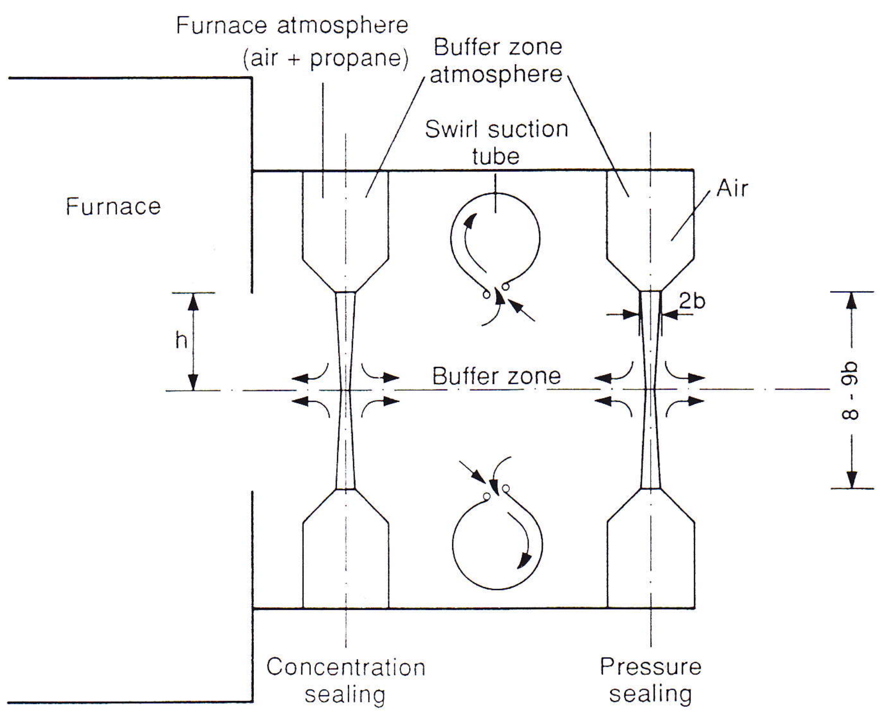

Fig. 3. Schematic of test arrangement to investigate the efficiency of the new sealing device (width of furnace opening = 900 mm).

Since the pressure difference against ambient inside the furnace was chosen to be relatively high ($\Delta p = 50$ Pa), pressure sealing in addition to concentration sealing was used. The buffer zone between the two sealing nozzle units was vented using a swirl suction tube. Having an almost constant suction force over the whole width of the arrangement, which is typical for swirl suction tube, is of advantage for venting the buffer zone.

The furnace atmosphere was simulated by introducing propane as the tracer gas. The propane concentration at various positions between ambient and furnace was measured using a flame ionization detector (FID).

6. Results and discussion

The first case considered for numerical prediction was the hydrogen–nitrogen jet flow. The N_2 inlet velocity was $V_2 = 10$ m s^{-1} and the H_2 inlet velocity was taken to ensure that the two half-jets had the same momentum flux at the nozzle exit, which in the present case corresponds to $V_1 = 37.3$ m s^{-1}. This is shown in Fig. 4, where a plane distribution of the velocity vectors is depicted.

Comparing, for the case of hydrogen–nitrogen, the flow patterns resulting from equal momentum fluxes (Fig. 5(a)) and equal velocities (Fig. 5(b)) at the nozzle exit, it can be concluded that when the condition of equal momentum flux is not ensured, the flow field centreline is deflected, thus yielding a lower sealing efficiency. This problem is particularly acute for the cases where the two incoming fluids have rather different densities, as in a typical furnace application, where one half-jet is taken from the furnace and the other from the ambient.

Figure 6 shows the horizontal distribution of air molar fraction, f_1, for different values of the distance above the impingement surface in the case of the air–nitrogen jet and for $h/2b = 4.6$. The sealing efficiency varies with the distance to the impingement surface. The lowest sealing efficiency was obtained near the impingement surface, increasing gradually with the distance away from the surface.

For the cases $y/h = 0.12$ and 0.84, near the $x = 0$ location, a small peak in the air molar fraction distribution can be observed. The existence of this peak may be due to the fact that a finite computational domain has been considered, which causes a large-scale recirculation zone, thus reinforcing the convective transport from the region of higher mixing.

The influence of nozzle height on the air molar fraction horizontal evolution can be analysed in Fig. 7, where a comparison is made for the air–nitrogen jet, for different values of $h/2b$ and for two locations: one near the impingement surface ($y/2b = 0.05$) and the other at half-jet height. The sealing efficiency decreases with increasing values of h for both locations. However, this effect is more evident for the less favourable region near the impingement surface (Fig. 7(a)).

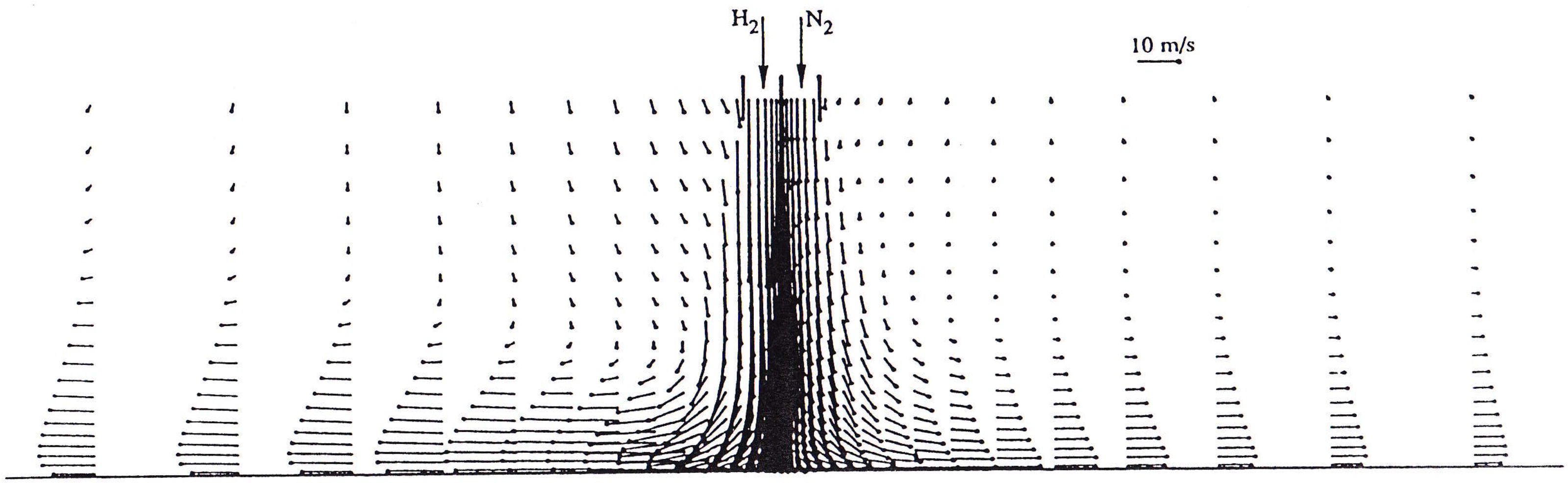

Fig. 4. Velocity vectors in a plane of the hydrogen–nitrogen jet flow ($V_1 = 37.3\ \mathrm{m\ s^{-1}}$; $V_2 = 10\ \mathrm{m\ s^{-1}}$).

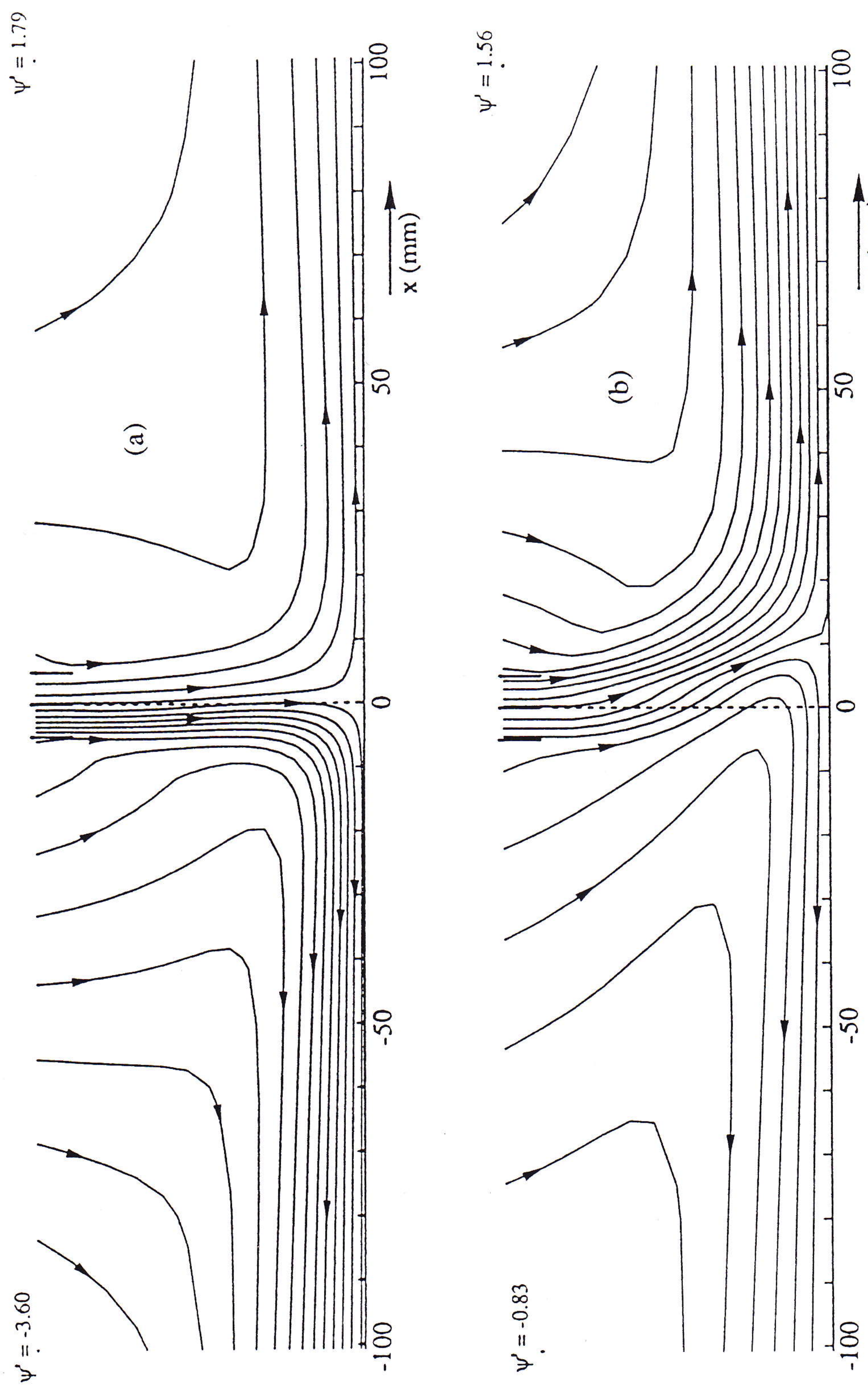

Fig. 5. Flow streamlines in a plane of the hydrogen–nitrogen jet flow ($\psi' = \psi/2bV_2$). (a) $V_1 = 37.3$ m s^{-1}, $V_2 = 10$ m s^{-1}; (b) $V_1 = V_2 = 10$ m s^{-1}.

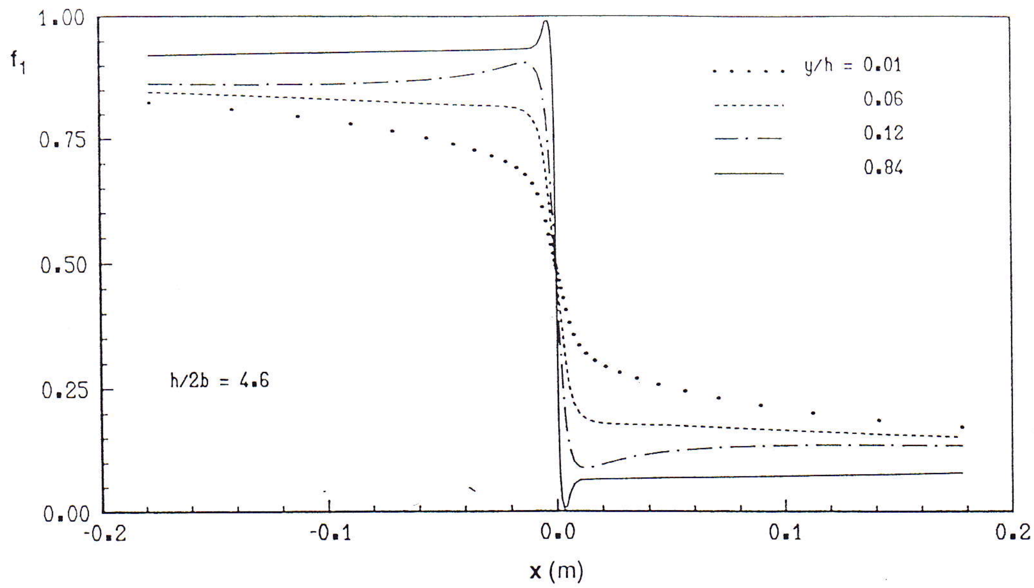

Fig. 6. Horizontal distribution of air molar fraction for different values of the distance above the impingement surface. Air/N_2 jet, $h/2b = 4.6$, $V_1 = V_2 = 10$ m s^{-1}.

To study the effect of fluid nature on the sealing efficiency, molar fraction distributions similar to the preceding ones may lead to misleading interpretations when the fluid densities are rather different, as for the H_2/N_2 jet. In this case, when $V_1 = 37.3$ m s^{-1} the H_2 presence is over-predicted because its molar flow rate at the nozzle exit is much higher than that of N_2. To overcome this problem, a direct comparison of the mass flow rate of component 1, which flows from the sub-domain $x<0$ to $x>0$, is performed. This flow rate is designated by $\dot{m}_1$ and is formed by two terms: a convective contribution, $\dot{m}_{1c}$, and a diffusion contribution, $\dot{m}_{1d}$, which can be calculated by

$$\dot{m}_1 = \dot{m}_{1c} + \dot{m}_{1d} \tag{11a}$$

$$\dot{m}_{1c} = \int_0^h \rho c_1 U \, \mathrm{d}y \tag{11b}$$

$$\dot{m}_{1d} = \int_0^h -D \frac{\partial(\rho c_1)}{\partial x} \, \mathrm{d}y \tag{11c}$$

where c_1 is the mass fraction of component 1, ρ is the mixture density, D is the local diffusion coefficient and U is the x-component velocity. The knowledge of $\dot{m}_1$ allows the calculation of the "sealing efficiency", η, which can be defined as

$$\eta = \left(1 - \frac{\dot{m}_1}{\dot{m}_{1\text{in}}}\right) \times 100\% \tag{12}$$

where $\dot{m}_{1\text{in}}$ is the mass flow rate of component 1 at the nozzle exit.

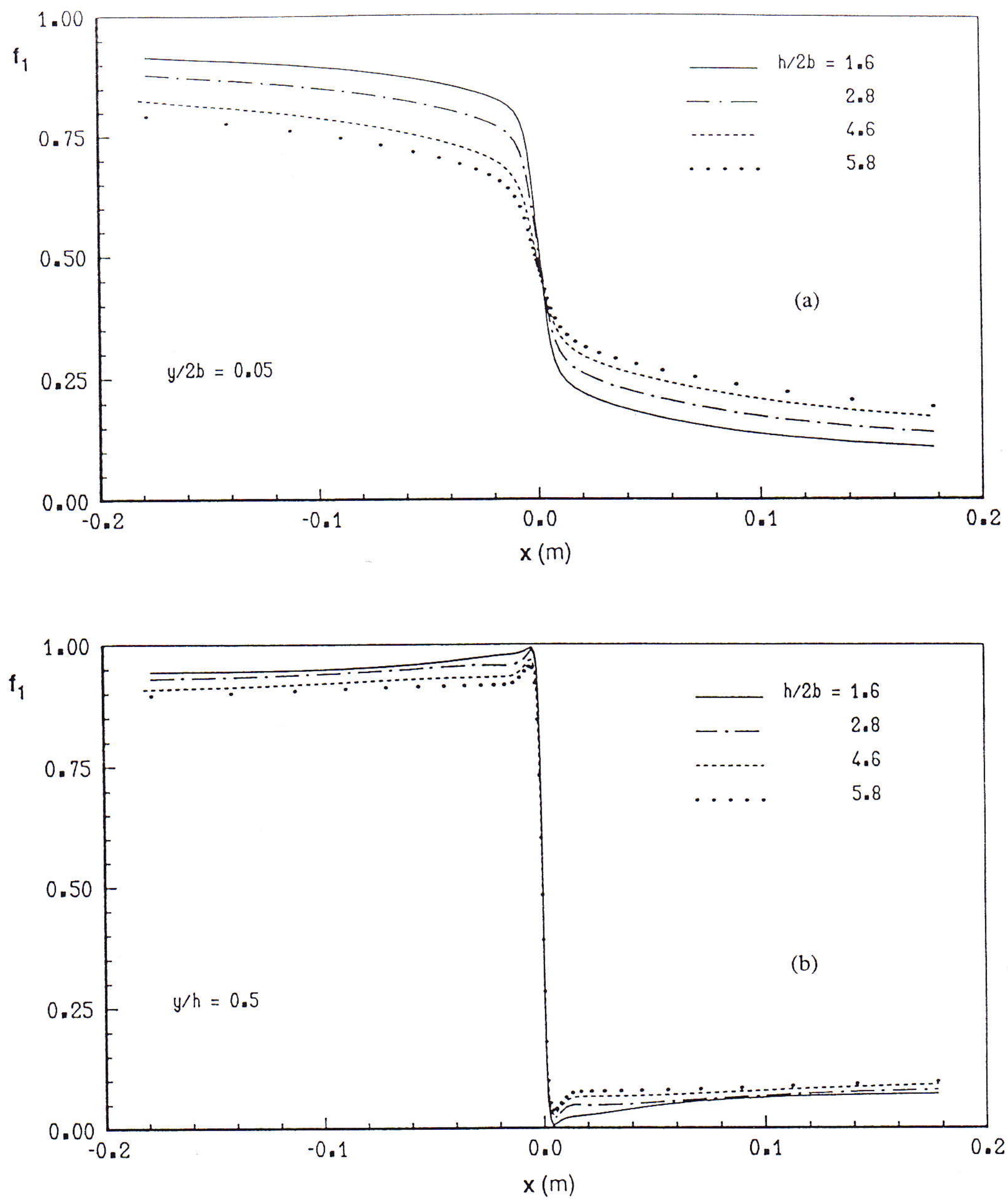

Fig. 7. Air/N_2 jet. Influence of nozzle height on air molar fraction horizontal evolution. $V_1 = V_2 = 10$ m s^{-1}. (a) $y/2b = 0.05$; (b) $y/h = 0.5$.

From the analysis of Table 2 it can be concluded that the sealing efficiency decreases with an increase in the difference between the density of the fluids. On the other hand, the results presented in Table 2 confirm that a better sealing effect is obtained for smaller distances from the nozzle to the impingement surface. These results stress the need to ensure the same flux momentum of the two half-jets at the nozzle exit.

Figure 8 shows a typical result of concentration measurement. The propane concentration measured in the centreline of a simulated strip is plotted against

TABLE 2

Sealing efficiency for some of the cases studied

Fluid 1/fluid 2	$h/2b$	V_1 ($m\ s^{-1}$)	V_2 ($m\ s^{-1}$)	η (%)
H_2/N_2	4.6	37.3	10	82.1
H_2/N_2	4.6	10	10	72.2
Air/N_2	4.6	10	10	89.5
Air/Air	1.6	10	10	97.0
Air/Air	4.6	10	10	89.9

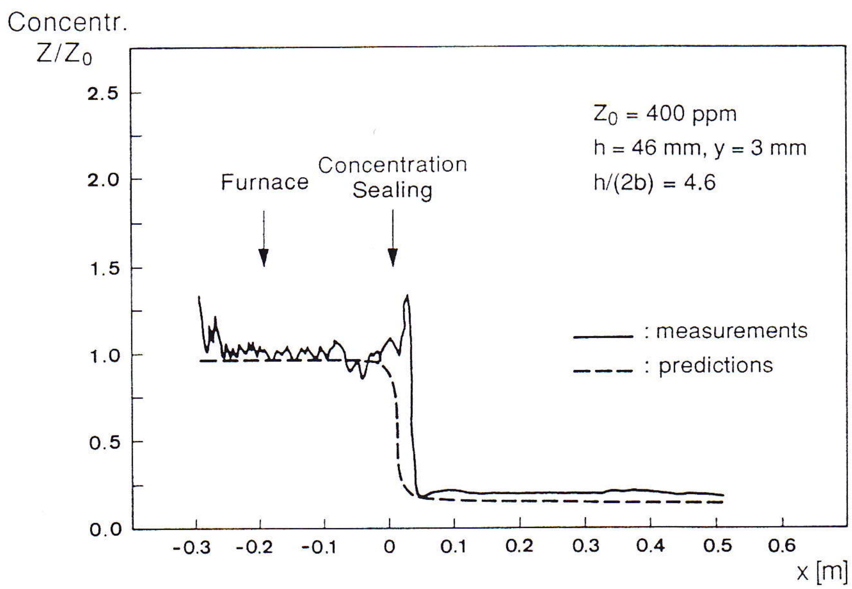

Fig. 8. Concentration of tracer gas in the centreline of the furnace entrance.

the strip direction. The concentration level at the furnace atmosphere was kept at approximately 400 ppm. The background propane concentration of the ambient air, which is due to leakages elsewhere in the furnace walls, grows slightly from 70 ppm to 80 ppm during the test run. The efficiency of the sealing device is clearly seen by the almost step-like decrease in propane concentration at the position of the concentration sealing. The dashed line represents the corresponding numerical prediction, thus showing a very good agreement between calculations and measurements. The slight difference near $x=0$ is due to an experimental uncertainty on the probe location.

Figure 9 shows a typical pressure distribution along the centreline of the sealing unit. It should be noted that the buffer zone exhibits almost ambient pressure. Thus, concentration sealing acts at the same time as pressure sealing, even at $\Delta p = 50$ Pa furnace pressure. Usually furnace pressures are smaller. In

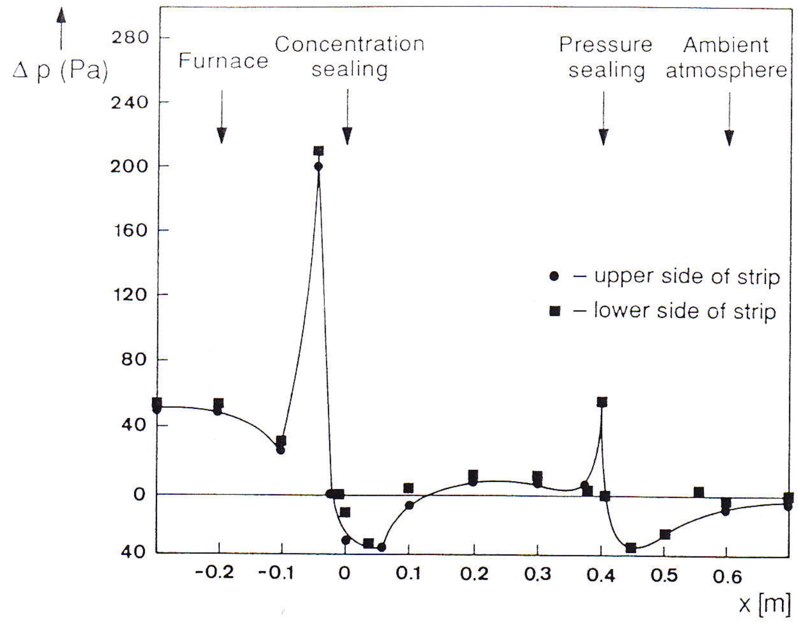

Fig. 9. Distribution of static pressure on a strip-like material in the furnace entrance.

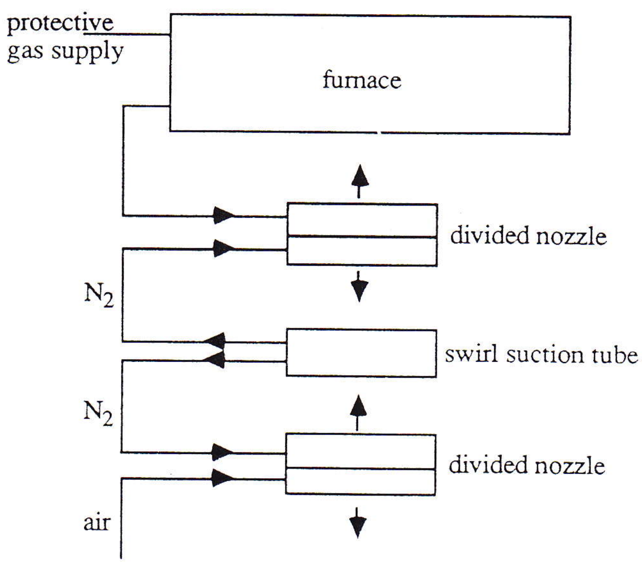

Fig. 10. Schematic of a sealing device using N_2 as the buffer gas.

those cases, concentration sealing may be used at the same time as pressure sealing.

For critical cases, where the density of the furnace atmosphere is extremely different from the density of ambient air, or if oxygen penetration into the furnace has to be prevented at all costs, a cascade-like concentration sealing may be used. A typical arrangement is shown in Fig. 10. The buffer gas extracted by the swirl suction tube is fed to the half-nozzles neighbouring the buffer zone. The furnace atmosphere is only used in one half-nozzle. The volume flows may be adjusted in such a way that only a very small leakage between the furnace atmosphere and the buffer zone and between the buffer zone and ambient occurs.

7. Concluding remarks

The new concentration sealing with a divided slot nozzle is very effective, leading to a step-like concentration gradient between chamber atmosphere and ambient.

The numerical method presented in this work provides a very useful and reliable theoretical analysis of the aerodynamic sealing effect obtained with such a device. Numerical predictions have stressed the need to ensure the same flux momentum in the two half-jets of the nozzle exit. For a fixed nozzle height, the leakage effect is seen to increase with decreasing distance to the impingement surface. Conversely, an increase in the nozzle height worsens the sealing effect. Sealing efficiency is negatively affected by the presence of fluids with high density differences.

Critical conditions may require a cascade-like concentration sealing structure.

For most practical applications the same device may be used as pressure sealing as well as concentration sealing.

References

1 A. Esteban and H. Colin de Verdier, Vertikale Durchlaufanlage zum Glühen von Messing und Kupferbändern, Gas Wärme Int., 21 (1972) p. 42.
2 H.-W. Kuster, Strahlabdichtungen von Durchlaufwärmebehandlungsanlagen mit schutzgasatmosphäre, Doctoral Dissertation, RWTH Aachen, West Germany (1983).
3 H. Elbanna and J.A. Sabbagh, Interaction of two nonequal plane parallel jets, AIAA J., 25 (1987) 12.
4 C. Kramer and H.J. Gerhardt, Gasstrahlabdichtung, German Patent P 37 43 598.1 (Dec. 1989); Apparatus for contactless sealing of an opening against emerging or entering gas, U.S. Patent No. 4.894, 009 (Jan 1990).
5 W.P. Jones and B.E. Launder, The prediction of laminarization with a two-equation model of turbulence, Int. J. Heat Mass Transfer, 15 (1972) 301.
6 B.E. Launder and D.B. Spalding, The numerical computation of turbulent flows, Comput. Meth. Appl. Mech. Eng., 3 (1974) 269.
7 A.D. Gosman and W.M. Pun, Calculation of recirculating flows, Lecture Notes, Dept. Mech. Eng., Imperial College, London, 1974.
8 D.B. Spalding, A novel finite difference formulation for differential expressions involving both first and second derivatives, Int. J. Num. Meth. Eng., 4 (1972) 551.
9 L.S. Caretto, A.D. Gosman, S.V. Patankar and D.B. Spalding, Two calculation procedures for steady, three-dimensional flows with recirculation, Proc. 3rd Int. Conf. Num. Fluid Dynam., Springer-Verlag, New York, 1972, p. 60.